Exploring Capacitance and Non-Linear Electrokinetics in Nanopores Yields Insight into Single Molecule Recordings

Nasim Farajpour[1,δ], Y. M. Nuwan D. Y. Bandara[1,δ], Vinay Sharma[2], Lauren Lastra[1], Kevin J. Freedman[1]*

[1]Department of Bioengineering, University of California, Riverside, 900 University Ave., Riverside, CA 92521, USA

[2]Department of Biosciences and Bioengineering, Indian Institute of Technology Jammu, NH-44, Jagti, Jammu, J & K, 181221 India

[δ] Equal Contributions

*Correspondence to: Kevin J. Freedman, Department of Bioengineering, University of California, Riverside, 900 University Ave., Riverside, CA 92521, USA.

E-mail: kfreedman@engr.ucr.edu

Abstract

The pervasive model for a solvated, ion-filled nanopore is often a resistor in parallel with a capacitor. Although the simple model suggests that ionic current can flow through both components, under voltage-clamped conditions, capacitive current *should* be negligible. However, non-linear electrokinetics routinely predict voltage and capacitance fluctuations that can lead to otherwise anomalous current transients. We aimed to test the hypothesis that voltage and/or capacitance can fluctuate despite distant electrodes being clamped at a specified voltage. The first supportive piece of evidence for this theory is the appearance of *negative* capacitance within the nanopore sensor which is characterized by long equilibration times and is observed only under millimolar salt concentrations. Next, we used the transient occlusion of the pore using λ-DNA and 10-kbp DNA to test whether events are being attenuated by this purely ionic phenomenon. We conclude the study with a new interpretation of molecular translocations which is not only based on the pulse-like resistance changes but rather a complex and non-linear pseudo-steady state that changes during molecular transit.

Introduction

Non-linear electrokinetic phenomenon is routinely used to explain otherwise anomalous data produced by electrochemical cells[1], ionic liquids[2], nanofluidic devices[3,4], and other systems[5-7]. The classical Poisson-Nernst-Planck and Navier-Stokes equations represent a useful approximation of current and ionic concentrations however tends to deviate from experiments under (1) crowded conditions and (2) strong surface interactions[8-10]. Although both 1 and 2 describe a nanopore filled with an electrolyte, the impact of non-linear electrokinetics on single molecule sensing experiments has not been explored. Although membrane capacitance is routinely studied as a source of noise, the electric double layer (EDL), which is composed of both Stern and diffuse layers, and are described by the Gouy-Chapman-Stern (GCS) model[11], also contributes capacitance that is distinct from the membrane (e.g. solid-state) capacitance. More importantly, the EDL capacitance is ion-specific and concentration-dependent which are routinely varied within nanopore experiments[8,12,13]. Since capacitive elements are capable of storing and releasing charge, they are important to consider when making ultra-small (i.e., femto-ampere) current measurements at the nanoscale interface. Nanopipettes, in particular, are well-suited for studying non-linear ionic phenomenon since the glass walls are highly charged and the geometry confines the ions and hinders diffusion to virtually one axis[14].

Electrical circuit equivalents, such as resistive and capacitive (RC) components, have routinely been used to model ideal charge transport in ionic systems[15,16]. The nanopore field has utilized these models to help understand the concepts of access resistance[17], sensing zone[18], capture radius[19], and capacitive noise[20,21]; the latter of which has been the theoretical basis for low noise nanopore systems[22]. However, these models ignore certain ionic phenomenon such as charge accumulation and recombination effects[23-26]. While the resistive nature of a nanopore is undisputed, the capacitive components of the nanopore system are undoubtedly more complex. Some capacitive phenomenon (e.g. “mem-capacitance”) are only revealed through simulations[27] which are not limited by bandwidth-limited instrumentation. Broadly, capacitive current can fall under two categories: (1) leaky capacitance wherein the voltage is not changing ($\frac{dV}{dt} = 0$) yet current can still traverse the capacitor, and (2) the more canonical capacitance wherein current only flows when there is a voltage change ($\frac{dV}{dt} \neq 0$). Leaky capacitance is mentioned here since

the EDL can both store charge as well as conduct charge along the interfacial surface[28]. Since the EDL can contribute to the conduction of ions through the nanopore, a leaky capacitor model may be fitting in some situations, such as low (mM) salt conditions. In its simplest form, the current through the RC circuit[21,29] can be expressed as:

$$\mathrm{i} = i_C + i_R = \mathrm{C}\,\frac{\mathrm{dV_C}}{\mathrm{dt}} + \frac{\mathrm{V_R}}{\mathrm{R}} \qquad \text{Eq. 1}$$

where C is the effective capacitance of the nanopore walls, R is the resistance of the nanopore, V_R is the voltage across the resistor, and V_C is the voltage across the capacitor. When considering the magnitude and sign of each current source, it is also important to consider negative capacitance and variable capacitance. Recently, the appearance of negative capacitance, meaning that the stored charge (Q) decreases with increasing voltage (V), has been reported in ionic systems[27,30,31]. The characteristic feature of negative capacitance is that the equilibrium (i.e., resistive) current is higher than the combined current (i.e., resistive and capacitive combined). Furthermore, while simple capacitors routinely do not change their capacitance, the same may not be true for ionic systems (e.g., ions could be stripped from a surface via a transverse potential or through ionic species' concentration variation[8]). Therefore, a more general form of current through a capacitor, considering capacitance variability, is:

$$\mathrm{i}_C = \mathrm{C(t)}\frac{\partial V(t)}{\partial t} + V(t)\frac{\partial C(t)}{\partial t} \qquad \text{Eq. 2}$$

From Eq. 2, transient current stemming from a capacitor can be produced by two sources: voltage fluctuations and capacitance fluctuations[32-35]. Justification for capacitance fluctuations is based on (1) EDL capacitance being concentration-dependent[8,36], and (2) concentration polarization which leads to charge enrichment and depletion[1,32-34]. Justification for voltage fluctuations within the nanopipette is based on several theoretical works[12,13,37] as well as the non-zero space charge density that appears within the nanopipette[38]. Despite global electro-neutrality being conserved, local neutrality can become unbalanced in nanofluidic systems[37]. Therefore, we propose that excess cations inside the nanopipette can change the voltage distribution (according to Poisson's equation). Since the voltage "seen" by the electrodes determines how much current to inject (and measure), the concentration profile of ions is critically important to understanding

current recordings. The hypothesis that charge accumulation can cause local potentials to develop over time is necessary to make the derivative of voltage non-zero[35,39,40].

Throughout this study, the properties of the capacitor and the circuit architecture itself will be explored. We postulate that the fixed charge on a substrate and the relatively fluctuating transport of anions and cations opens the door to *local* violations of electroneutrality[35,41], the build-up of electric potential, and capacitive currents. The parallel circuit architecture also does perfectly match the physical system since the nanopore is the only current path between the electrodes. In other words, if ions are momentarily stored at the quartz-electrolyte interface, the same ions will also traverse the pore when released. Whereas in a truly parallel circuit, capacitive current bypasses the resistor and has a truly unique current path. Similarly, a resistor in series with a capacitor is also unrealistic since the capacitor will block all steady state current flow eventually; except in the case of a leaky capacitor. Here, we use nanopipettes to explore EDL capacitance effects at low (1-10 mM) and asymmetric (1 M/4 M) salt concentrations. Salt gradients were included here due to several reports of non-linear electrokinetic behavior[1,8,42,43]. Both current-voltage (IV) data and translocation data will be used to explore the nature of capacitance in nanopipettes and how the capacitance may influence the collection of single molecule data.

Results and Discussion

Current-Voltage (IV) Relationships Within a Nanopipette

Nanopipettes were fabricated from laser heating quartz capillaries and pulling them to nanoscale conical tips. Using high salt conditions (1 M KCl, pH 7.4) and a 30 nm pore, a voltage-sweep was performed from -500 mV to +500 mV (100 mV increments, **Fig. 1a**). The ionic current recorded at positive and negative voltages did not show strong rectification and the capacitive current spike occurring at ~2 seconds exhibited positive capacitance (i.e., an increase in current when $\frac{dV}{dt} \neq 0$). The first 20 ms (after the voltage switch) was extracted and the current trace's final value (i.e., the resistive current) was subtracted to yield only the capacitive current (see Methods). While the current magnitude at the time of the voltage switch scales with the magnitude of the voltage change, the decay constant should be relatively constant and governed

by both the resistance of the pore and the capacitance of the glass. Exponential decays ($I = I_o e^{-rt}$) were fitted to each of the capacitive current traces and the mean decay rate, r, was found to be 484 ± 26 s^{-1} across the voltages tested. Since capacitive current typically leads to a decrease in current over time, if the current decayed towards a higher current magnitude, the sign (+/-) of the decay rate was adjusted to a negative value to indicate the appearance of negative capacitance. Although the term 'negative capacitance' is used here, it will simply refer the appearance of negative capacitance which could be caused by either capacitance or the derivative of voltage being negative.

At low salt conditions (10 mM KCl, pH ~7.4) negative capacitance is observed at both small (i.e., 30 nm) and large (250 nm) pore sizes (albeit at negative voltages only, **Fig. 1b**). Pore sizing details are provided in the **Supplemental Information**. The decay rates were extracted at each voltage and a similar voltage dependence was observed wherein the notable first negative decay rate occurred at -200 mV. While the transition from positive to negative decay rates were not significantly different, the timescale of the decay, or discharge, of the capacitive current was notably different between all three experiments. It should be noted that larger decay rates indicate a faster decay of current towards its equilibrium. However, the value of the decay rate, especially for low salt conditions, is not constant throughout a single voltage trace. This means that the decay rate associated with capacitance changes over time, becoming smaller as time passes. This is observed in each of the insets in **Figure 1b** and **Figure 1d**. Interestingly, the decay rate for the smaller pore size (30 nm, -500 mV trace) remained high for a longer time period after the voltage switch compared to the larger pore size (250 nm, -500 mV trace); for the larger pore, the decay rate drops to nearly zero after about 1 second. Therefore, the pore size seems to play a role in how long the capacitive current takes to decay to zero and may be related to hindered diffusion of the ions since the time to reach equilibrium is slower for smaller pores.

Elaborating on the negative capacitance effects observed at negative voltages, it is clear that the resistive current is negative and capacitive current is positive (counteracting the negative resistive current). In order for the capacitive term ($C\frac{dV}{dt}$) of current to produce positive current, the value of C must take on a negative value since $\frac{dV}{dt}$, in principle, is negative as well (e.g., $\frac{dV}{dt} = \frac{V_2 - V_1}{t_2 - t_1}$ where t_1, t_2, V_1, and V_2 are the time and voltage during a voltage switch). Therefore,

C appears to be negative in the experiments shown here. Although no literature could be found on Debye layer dynamics in a transverse electric field, it at least was conceivable that higher voltages could strip weakly bound cations from the quartz surface. If so, the fact that charge is reduced as voltage is increased coincides with the definition of negative capacitance. The alternative is that capacitance is positive and after the initial voltage bias, relatively slower charge depletion phenomenon produces surface potentials which could alter the voltage bias at the pore ($V_{pore}=V_{applied}+V_{surface}$). Taking the derivative, we obtain $\frac{dV_{pore}}{dt} = \frac{V_{surface}}{dt}$ where $\frac{dV_{applied}}{dt} = 0$. Under this theory, the voltage across the pore is dynamic and could take on both positive and negative values during charge enrichment and depletion, respectively. A third possibility also exists in which the capacitance is variable leading to an additional source of current modulation ($V\frac{dC}{dt}$). This is probably the least likely scenario since the intrinsic ability to store charge is unlikely to change within the nanopipette. Two simple circuit models are proposed: a variable resistor in parallel with a variable capacitor (model 1), and a variable resistor in parallel with a standard capacitor which can take on positive and negative values (model 2). Schematics and governing equations for the current through each circuit is shown in **Figure 1** (f-g). The sign of each term is particularly important since the capacitive terms must be positive in order to counter the negative resistive current (strictly under V<0 conditions) in order to explain the observed negative capacitance. The variable resistance is only applicable for translocation events wherein the resistance of the pore changes, otherwise we can assume that the resistor's current is constant.

In terms of the longer than anticipated timescale of the capacitive current, two contributions can be considered: the charge relaxation time, which is usually found by calculating the Debye time ($\tau_D = \frac{\lambda_D^2}{D}$), and the concentration diffusion time ($\tau_C = \frac{L^2}{D}$)[13]. For typical values of the Debye length (λ=1-10 nm) and diffusion coefficient ($D=10^3$ $\mu m^2/s$), the Debye time ranges from 1-100 ns. Conversely, we suspect that ions will need to diffuse several hundred microns in order to dissipate their charge[14]. As an example of the confinement experienced by an ion, consider a 10 nm pore with a typical outer cone angle of 10 degrees. Even if an ion travelled five microns inside the taper (starting from the tip), the inner glass confinement is still roughly 440 nm (i.e., internal diameter). If a diffusional length, L, of 50 μm

is used, the relaxation time would be 2.5 seconds which is roughly on the same scale as the current transients found here. The hindered diffusion hypothesis also would also explain why larger pores seem to equilibrate faster (**Fig. 1d**). This would also suggest that symmetric pores which do not have the tapered geometry would not display the same current transients. The results are also distinct from concentration polarization which is typically observed as the electrolyte conductivity (i.e., specifically within the taper of the nanopipette) decreasing over time at negative applied voltages and increasing over time at positive applied voltages.

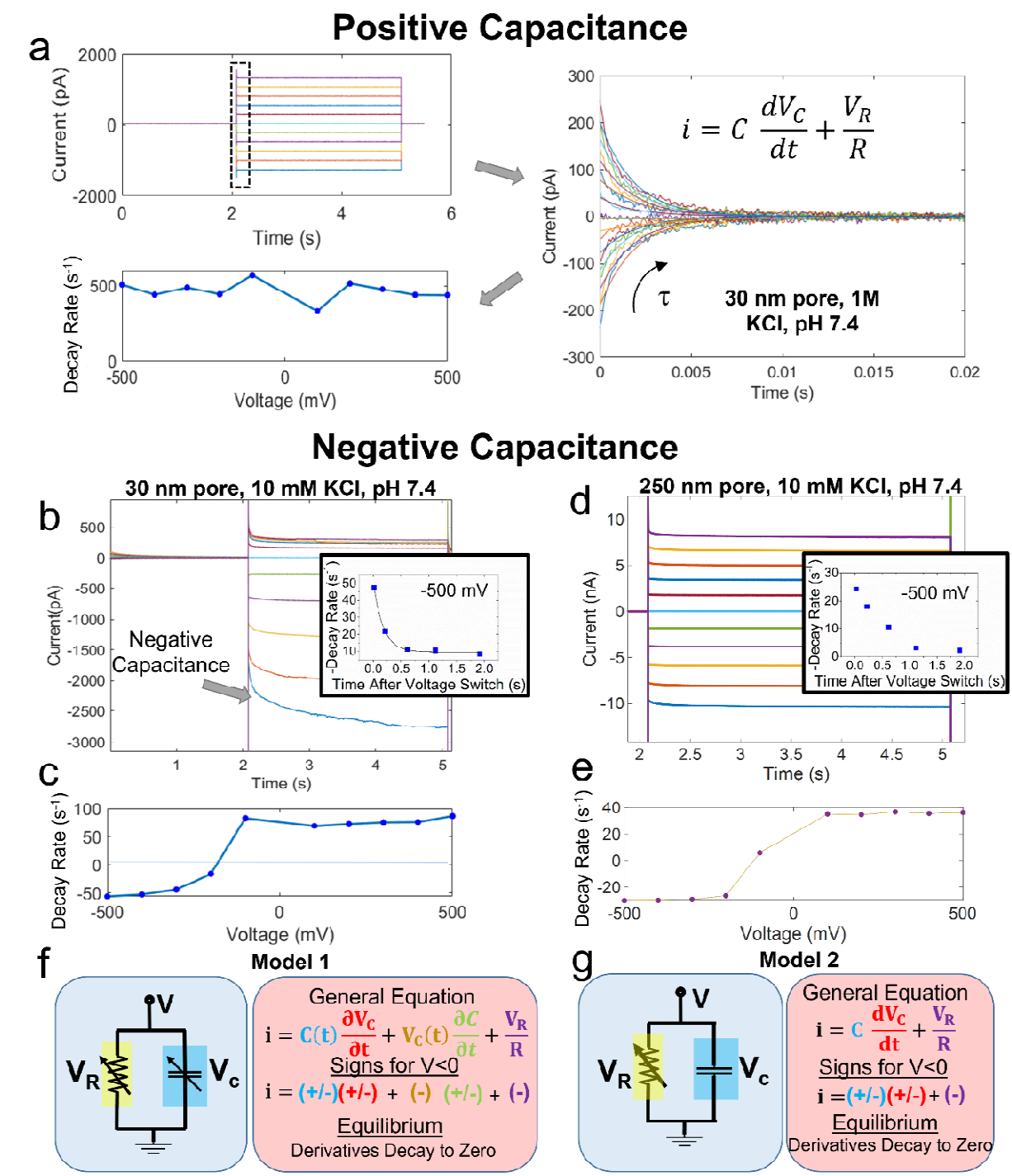

Fig. 1. (a) Current-Voltage (IV) relationship for a ~30 nm pore in 1 M KCl (pH 7.4). The first 20 ms of data with the equilibrium (resistive) current subtracted is also shown. Exponential fits are shown for each voltage and the corresponding time constant (s^{-1}) are plotted as a function of voltage. (b) IV relationship for a similarly sized pore (30 nm) in 10 mM KCl (pH 7.4). Inset:

the decay rate at various time points for the -500 mV voltage switch. (c) The decay rate as a function of voltage for the first 20 ms of each voltage switch (from 0 V to the specified voltage on the x-axis). (d) IV relationship for a 250 nm pore filled with 10 mM KCl (pH 7.4). Inset: the time constant at various time points for the -500 mV voltage switch. (e) The decay rate as a function of voltage for the first 20 ms of each voltage switch. (f-g) Schematic circuit model and corresponding equations and properties for model 1 and model 2, respectively. Both model 1 and model 2 have a variable resistor and model 1 has a variable capacitor.

Based on the ionic theory for dynamic screening of a charged surface, we further investigated the dependence of negative capacitance on ionic concentration and pH; KCl concentration and pH both influence the zeta potential of the glass surface. Four separate pores were filled with the following buffers (symmetric on both sides): (1) 10 mM KCl (pH ~7.4), (2) 10 mM KCl (pH ~10), (3) 1 mM KCl (pH ~7.4), and 1 mM KCl (pH ~10). A wider voltage range of -1000 mV to +1000 mV was also used (**Fig. 2**). In comparing the four IV curves (particularly the -1000 mV trace which is the bottom blue trace), the lower salt (1 mM) exhibited less negative capacitance. Although 1 mM should have a higher zeta potential, less ions in solution also means that the rate of charging would be slower (i.e., 10-fold reduced flux of cations). For both 1 mM and 10 mM, increasing the pH led to a more prominent negative capacitance effect. Both the pH and salt dependence can be explained by a model in which the charging of the nanopipette is associated to cation flux and the surface charge (i.e., cation binding capacity of the surface). The localization of positive charge is thought to be a long-range interaction with the charged surface which may simply slow down the migration of cations in the confined tapered region. For example, the non-mobile cations next to the nanopipette surface (i.e., the compact layer, or Stern layer) are thought to remain attached to the glass throughout the voltage sweep. Using Coulomb's Law, the holding force of a cation to a single hydroxyl group (in the charged state) on the nanopipette surface, assuming a separation distance of 20 Angstroms, is 59 pN. Assuming a peak electric field inside the pore of 10^7 V/m, the Lorentz force or pulling force on the same ion is only 1.6 pN. Therefore, the layer of cations nearest to the surface are stationary despite the large pore electric field (i.e., for the voltages used here). However, the pH effects on the timescale of capacitive currents seems to allude to the surface

charge slowing down the migration of cations which we previously described as being diffusive in nature. Hindered cation diffusion may in fact be hindered through both confinement effects as well electrostatics.

Using the -1000 mV voltage trace (the bottom most current traces in **Fig. 2a-d**), the first 20 ms after the voltage switch was fitted to an exponential and the decay rate was extracted. As mentioned earlier, the first 20 ms always yielded the highest value of the decay rate before the decay rate itself, also falls to zero. The slow decay of the time constant at -1000 mV is evident by the long time it takes for the current to stabilize (>1 s in all experiments). The *initial* decay rate for each experiment at -1000 mV increased with higher pH values and decreased at the lower salt concentrations (**see Supplemental Information**). Capacitive current (i.e., the current transients) were obtained for each condition by subtracting the equilibrated current value (**Fig. 2e**). In both the 1 mM and 10 mM conditions, the initial capacitive current value was higher at pH 10 which we attributed to the higher charge storage capacity of the quartz surface caused by more hydroxyl groups being in the negatively charged state. In both the pH 7 and pH 10 conditions, the initial capacitive current was higher for the 10 mM salt concentration which we attributed to a higher flux of cations into the pore. The pH and salt concentration trends were consistent across all other voltage steps in which negative capacitance was observed (-300 to -900 mV) as well.

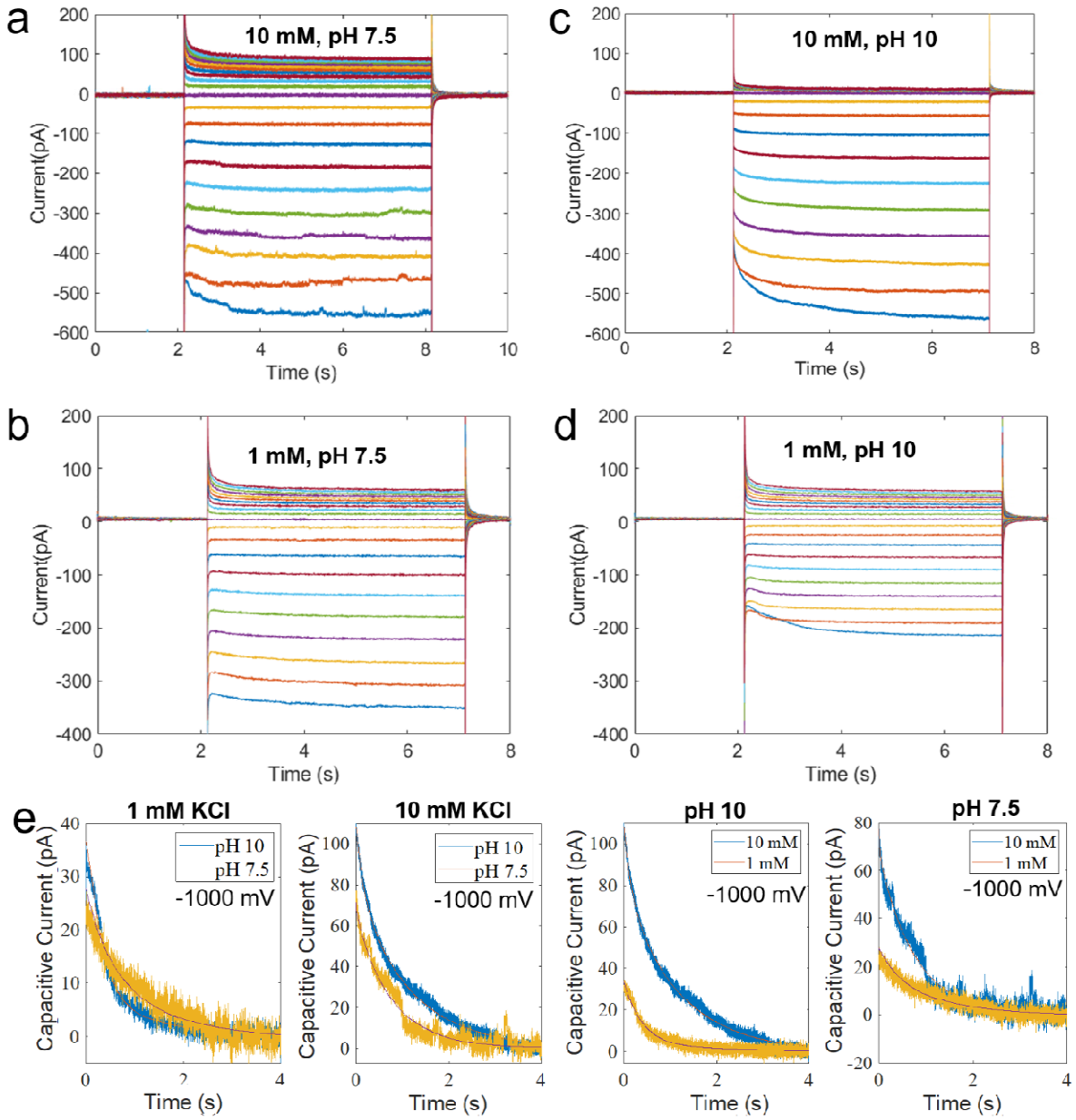

Fig 2. Current-Voltage (IV) relationships for four ~15 nm pores under different salt and pH conditions. (a-b) IV relationship for 10 mM KCl and 1 mM KCl for the voltage range -1000 mV to +1000 mV (100 mV increments) at pH 7. (c-d) IV relationship for 10 mM KCl and 1 mM KCl for the voltage range -1000 mV to +1000 mV (100 mV increments) at pH 10. (e) Current transients were isolated by subtracting the equilibrated (resistive) current leaving only the capacitive current behind. All traces were collected at an applied voltage bias of -1000 mV and show a salt and pH dependence.

Single Molecule Translocation Experiments at Low Salt

The term resistive pulse sensing implies that the resistance (R) of the nanopore is changed during molecular translocations and the capacitive current change is zero. However, to explain the observed effects up until now, one or more of the following conditions must apply to a voltage biased pore: (1) C<0, (2) $\frac{dC}{dt} \neq 0$, (3) $\frac{dV}{dt} \neq 0$. During a translocation event, a molecule such as DNA, typically occludes the ion flow and perturbs the ionic equilibrium of the pore. In all the experiments conducted here, DNA produced current enhancements (rather than current reductions) which we suspect is due to charge accumulation inside the tapered region of the nanopipette[38]. If the equilibrium is perturbed, the discharge of current should exhibit a decay rate governed by the RC time constant. Additionally, once DNA enters the pore, the DNA itself could store or eliminate ions and change the decay rate. If a decay of ionic current is observed in translocation events, the RC time constant during DNA entry and exit (event rise and fall time) could be helpful in elucidating the nature of capacitance in nanopores.

The prototypical nanopore experiment involves placing λ-DNA in one side of the nanopore (pore diameter in this experiment was approximately 20 nm, see Supporting Information) and applying a voltage bias. Here, DNA was placed in both sides of the nanopore and an I-V curve was recorded (**Fig. 3a-b**). Three notable observations can be made about the IV curve: (1) negative capacitance is observed at -500 mV and -400 mV, (2) the DNA event signatures at -500 mV and -400 mV seem to show a time constant associated with transition from an open pore to a blocked pore, and (3) DNA events are resistive at positive voltages and conductive at negative voltages. The first observation was reproducible and characterized all pores tested under 10 mM KCl. The second observation (i.e., evidence of a time constant within each event signature) has not been described in the literature to-date but seems to coincide with the negative capacitance effect observed during a voltage switch (both occurring at -400 mV in this pore). It was also clear from the current signatures (**Fig. 3c**) that if the event duration (i.e., dwell time) decreased, the current enhancement would not reach its maximum value (i.e. the events were attenuated in amplitude). A time constant associated translocation events implies that there could be an ionic lowpass filter in addition to the lowpass instrument filter which is routinely used to reduce noise (**Fig. 3d**). Finally, the third observation demonstrates an example of the translocation-direction dependence of event type (i.e., resistive versus conductive). At

positive voltages, the DNA outside the nanopipette translocate into the nanopipette. At negative voltages, the DNA inside the nanopipette translocate out of the nanopipette tip. Although the salt and DNA are the same, the event type is different for “in” versus “out” events. It should be noted that conductive events, in general, are far more likely at negative voltages and tend to have much higher signal to noise than resistive events at positive voltages (**Fig. 3b**). The prevailing theory that counterions on the DNA are responsible for conductive events seems unlikely since the DNA has the same counterions irrespective of the transport direction. Previous work proposed a theory for the nature of conductive events which is based on a flux imbalance between cations and anions[38]; namely that excess cations going into the pore yields conductive events which indeed would occur at negative voltages here. Further information about the DNA event properties such as current modulation depth and dwell time can be found in the Supplemental Information.

Two additional experiments were then conducted in which DNA starts inside the nanopipette, and a negative voltage bias (relative to the bath/ground) is applied to translocate DNA. At the pH of 7.4, events are slowed down by electroosmotic flow which opposes the electrophoretic transport of DNA. At this pH, event durations span a wider range compared to the lower pH of 6. It is evident that the dwell time of the DNA inside the pore has a direct impact on the current enhancement (**Fig. 3e and f**). At the lower pH of 6, all the events seem to have smaller current enhancements (**Fig. 3g and h**). At this stage, it is unclear whether events with small current enhancements are indeed attenuated or represent “false events”. False events are current modulations which do not ultimately result in DNA transiting the pore[44]. A full voltage sweep was performed to help elucidate which mechanism can best explain the data: attenuated or false events. Attenuated events should increase with voltage since the translocation time decreases with larger electrophoretic force whereas false events should decrease with increasing voltage since the ability to reverse from the pore is even less likely given the higher electrophoretic force. Our results (**see Supplemental Information**) indicate that the number of attenuated events increases with voltage which we suspect is due to a higher number of events being less than the critical dwell time (~1.5 ms).

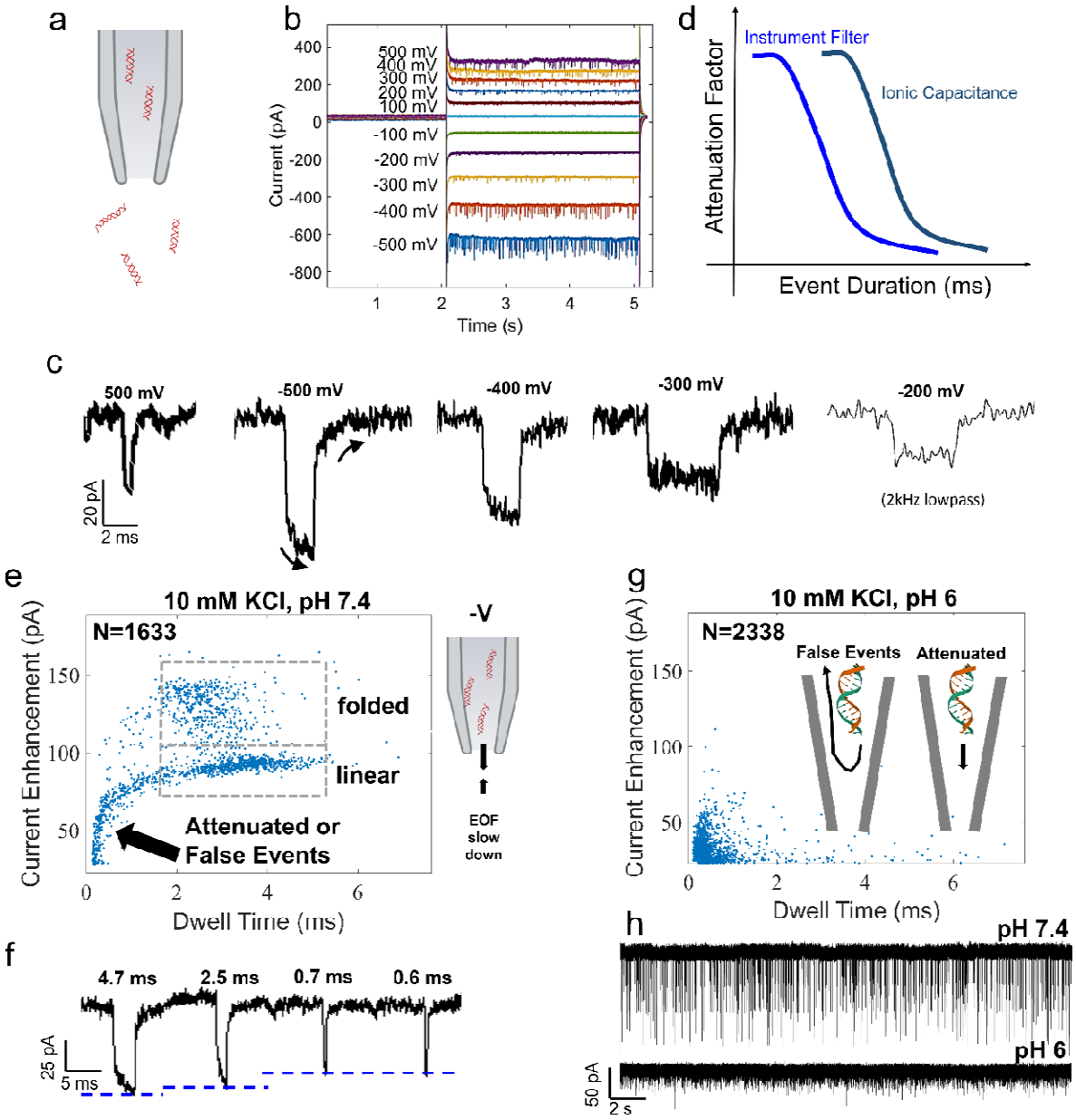

Fig. 3. (a) Schematic of experimental conditions (i.e. DNA location) for data in (b) and (c). (b) Current-Voltage (IV) relationship for the following condition located inside and outside the nanopipette: 500 pM λ-DNA, 10 mM KCl (pH 7). (c) Event signatures for the following voltages: +500 mV, -500 mV, -400 mV, -300 mV, and -200 mV. Unless otherwise noted, the instrument filter was a 10 kHz lowpass filter. (d) Schematic of the proposed attenuation curves for a 10 kHz lowpass filter and a filter of ionic origins (both a function of the event duration). (e) The peak current amplitude of each event (i.e. current enhancement) versus the dwell time for

each event. The analyte, λ-DNA, was only located inside the nanopipette with 10 mM KCl (pH 7.4) on both sides of the nanopipette and events were observed at negative voltages. The data in (e) was recorded at -400 mV. (f) Event signatures, each labelled with their dwell time, to illustrate the attenuation of the current enhancements. (g) Scatter plot of event properties (peak current enhancement and dwell time) for λ-DNA inside the pipette and with 10 mM KCl (pH 6) on both sides of the nanopipette. The data in (g) was recorded at -400 mV. (h) Long current traces for the data shown in (e) and (g) showing the differences in signal to noise and current enhancements induced by λ-DNA.

The theoretical basis for an ionic filter has not been established and therefore we sought to find the decay rate associated with DNA entering the pore and DNA exiting the pore. Once again, DNA was placed inside the nanopipette with 10 mM KCl (pH 7.4) on both sides of the pore (**Fig. 4a**). Using data obtained at a voltage bias of -500 mV, the event rise (DNA entry into the pore) and event fall (DNA exit from the pore) were fitted to an exponential. An average current trace across all events (n=625) representing the event rise and event fall is shown in **Figure 4b**. The event rise (DNA entering the pore) was decayed faster compared to the event fall (DNA exiting the pore); noting that the rise and fall designations are for conductive events. Less than 10% of events were filtered out due to variability in the traces which led to poor fitting of an exponential (e.g., **Fig. 4b** inset). The peak value for the decay rates were 5300 s^{-1} and 2500 s^{-1} for DNA entry and exit, respectively. Since the prototypical lowpass filter can be modelled as an RC circuit, and the time constant is equal to the product of the resistance and capacitance, the equivalent capacitance of the pore with and without DNA can be calculated. The resistance value of the pore was obtained from the I-V curve (negative voltages only due to rectification) and was found to be 1.3 GΩ. The resulting capacitance values were 123 and 304 fF for DNA entering the pore and DNA exiting the pore, respectively. Although the change in capacitance is clearly modulated by the presence of DNA, the ionic and/or molecular basis for the change in capacitance is unclear. The decay rate being faster for DNA events, compared to a voltage switch from 0V to -1V, for example, is likely due to the degree of perturbation of the ionic

species within the nanopipette (i.e., the ionic flux change due to DNA is small compared to the flux change due to a voltage switch).

In terms of the practicality of performing single molecule event detection, we sought to develop a theoretical framework for obtaining the minimum event duration that would result in no attenuation of the events. The equation that describes the relationship between the decay rate, time constant, and the effective rise time of a lowpass filter is: $\frac{1}{r} = \tau = \frac{T_r}{2.2}$, where T_r is the rise time (see Supporting Information for derivation). Using the two values of the decay rate, the rise times of the effective filter were found to be 880 µs (event fall) and 415 µs (event rise). While a typical filter has the same time constant for both the rise and fall of an event (minimum event duration without attenuation is $2\times T_r$), here the minimum event duration ($T_{critical}$) without attenuation is the summation of the rise (T_r) and fall (T_f) times (880+415=1295 µs). Using this threshold value, events were split into two groups based on the value of the dwell time (t_d). The current enhancements were distinctly different between the two groups (**Fig 4e**). The events with dwell times larger than 1295 µs showed two clear peaks corresponding to linear and folded DNA. The events that have dwell times less than 1295 µs has smaller current enhancements and no longer were able to resolve DNA folding.

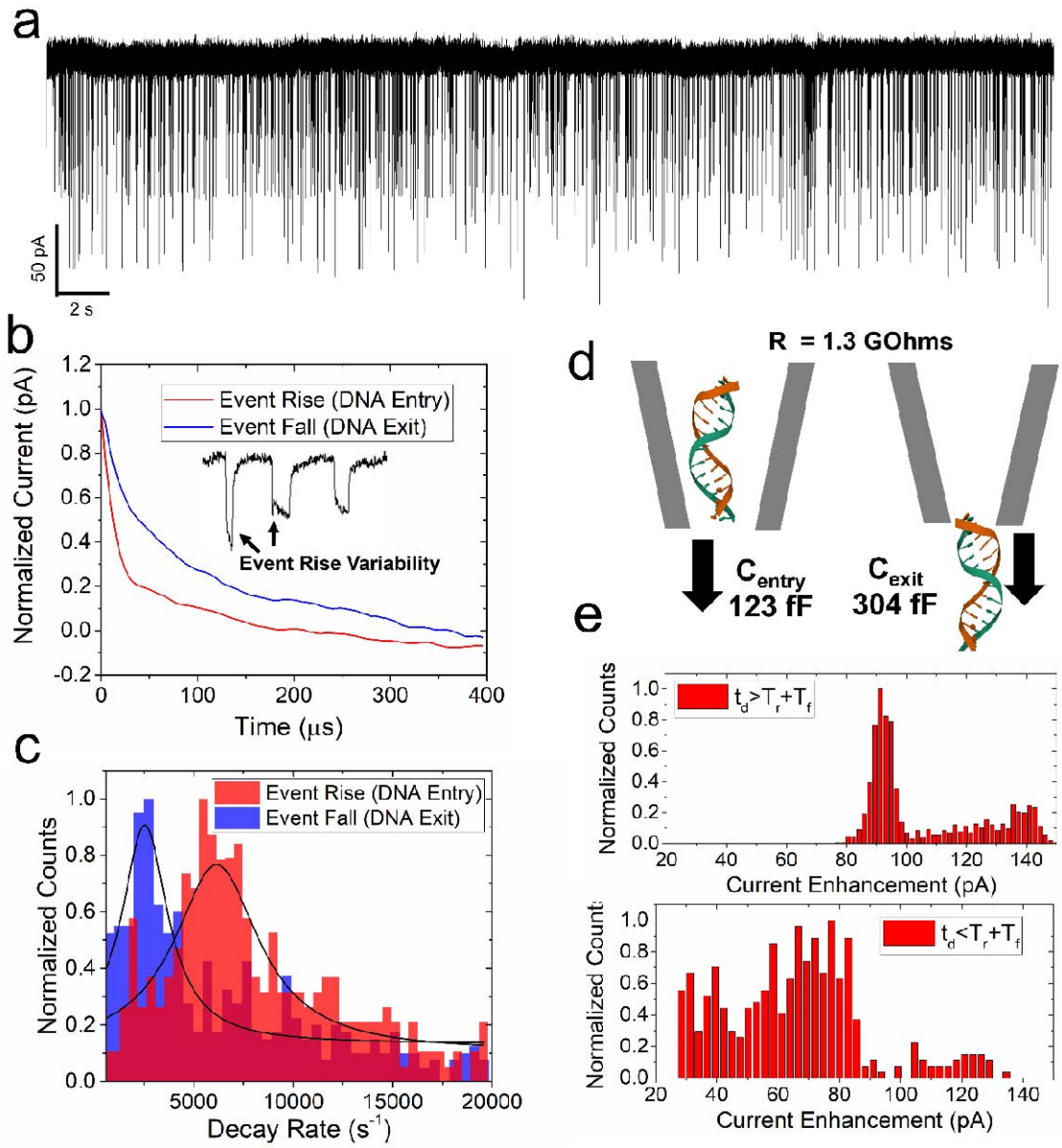

Fig. 4 (a) A long (50 s) current trace showing conductive events (500 pM λ-DNA) with symmetric 10 mM KCl (pH 7.4). The applied voltage bias was -400 mV. (b) Average of different sub-regions of λ-DNA current signatures (event rise and event fall averaged over 625 events). Inset: examples of event rise variability wherein DNA folding or attenuation can hinder the observation of ionic current time constant. (c) Histogram of the time constant extracted from each event's rise and fall. The ionic current decay towards its equilibrium value was fitted by an exponential and the time constant was extracted for each event. See Methods for more details. (d) Schematic illustration showing how the position of DNA inside the nanopipette seems to

impact the measured capacitance (i.e. RC constant) during the event rise and event fall. (e) Current enhancement histograms for events which have dwell times (t_d) above (top) and below (bottom) the critical event duration ($T_{critical}=T_r+T_f$). Below $T_{critical}$, attenuation of the current signature is expected.

Attenuated DNA events are shown in **Figure 5a** and examples are shown for three categories of DNA events: linear, partially folded, and fully folded. A core assumption of the attenuation theory is that DNA events will be attenuated roughly proportional to the measured dwell time of the DNA events. The equation that can be used to correct for attenuation is:

Eq. 3

$$\Delta I_{corrected} = \frac{\Delta I}{\mathrm{erf}\,(2.668 \times F_{LP} \times t_d)},$$

where F_{LP} is the cutoff frequency of the lowpass filter. The error function alone can also be used to generate an expected attenuation curve for various dwell times. Experiments were performed for voltage biases in the range of -200 mV to -1000 mV (10 mM KCl, pH 7.4). The data for the voltages -500 mV, -600 mV, and -700 mV are shown in **Figures 5b-d**. The error function was then used to generate the expected attenuation curves for the three DNA states: linear, partially folded, and fully folded. In all three DNA configurations, and all three voltages, the lowpass filter frequency (F_{LP}) which best fit the data was 500 Hz. This effective lowpass filter frequency is significantly smaller than the 10 kHz instrumentation filter that was used to reduce electrical noise.

A histogram of the current enhancements was generated for both the extracted ΔI and the corrected ΔI based on Equation 1 (**Figure 5e-f**). The extracted ΔI histogram lacked distinguishable peaks corresponding to the different configurations of the DNA. Furthermore, the events below 150 pA are entirely made up of the attenuated events and do not fit will with a single Gaussian population centered at the first peak located at 179 pA. Using Equation 3, all ΔI values were converted to $\Delta I_{corrected}$. The correction yielded three easily distinguishable peaks corresponding to linear (1), partially folded (2), and fully folded (3) in **Figure 5f**. A cutoff filter frequency of 500 Hz was used for the correction.

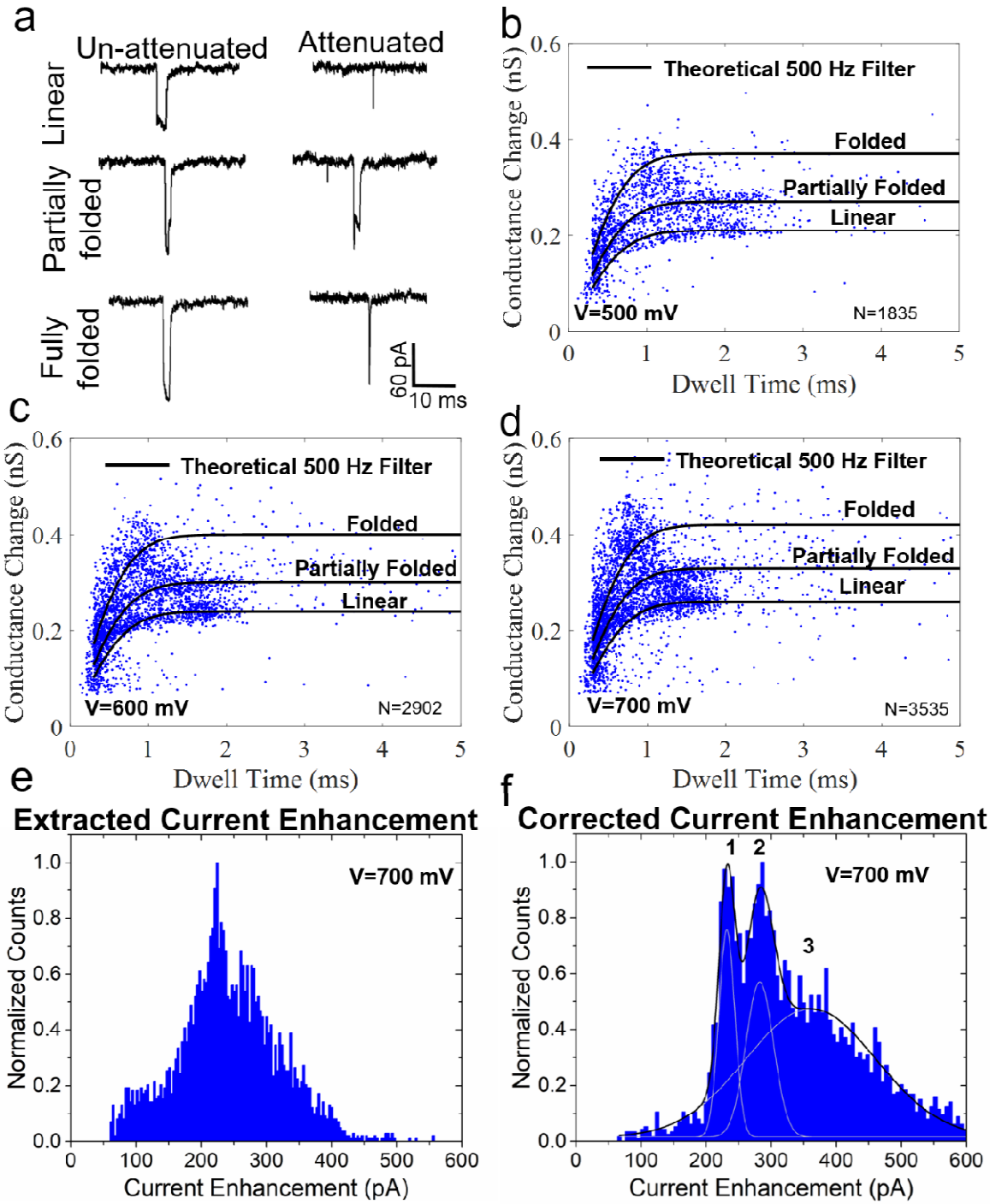
a
Un-attenuated
Attenuated
Linear
Partially folded
Fully folded
60 pA
10 ms
b
Theoretical 500 Hz Filter
Folded
Partially Folded
Linear
V=500 mV
N=1835
Conductance Change (nS)
Dwell Time (ms)
c
Theoretical 500 Hz Filter
Folded
Partially Folded
Linear
V=600 mV
N=2902
Conductance Change (nS)
Dwell Time (ms)
d
Theoretical 500 Hz Filter
Folded
Partially Folded
Linear
V=700 mV
N=3535
Conductance Change (nS)
Dwell Time (ms)
e
Extracted Current Enhancement
V=700 mV
Normalized Counts
Current Enhancement (pA)
f
Corrected Current Enhancement
1
2
3
V=700 mV
Normalized Counts
Current Enhancement (pA)

Fig. 5 (a) Characteristic event signatures for linear, partially folded, and fully folded events (left: un-attenuated events, right: attenuated events). Events were recorded -500 mV (electrolyte: 10 mM KCl, pH 8). (b-d) The conductance change ($\Delta I/\Delta V$) for λ-DNA at voltages -500 mV, -600 mV, and -700 mV, respectively. The black lines are the predicted attenuation curves for each DNA configuration assuming a cutoff frequency of 500 Hz. Note that all signals were recorded using a 10kHz lowpass filter. (e-f) Extracted and corrected current enhancement histograms for the voltage bias of -700 mV. Gaussian peak fitting was performed on (f) and shows three peaks corresponding to linear (1), partially folded (2), and fully folded (3).

Molecule-Specific Decay Rates at Asymmetric Salt Conditions

At low salt conditions, the translocation of DNA yielded current enhancements which were characterized by two different decay rates towards their equilibrium current values (i.e., the blocked current state, and the open pore current state). Another salt condition has also been found recently to produce current enhancements and occurs when there is a salt imbalance[45]. As opposed to 10 mM salt which exhibits strong electroosmotic flow that creates a flux imbalance, the asymmetric salt condition causes an asymmetric number of cations versus anions to enter the pore and can create non-linear effects[38]. Using 1 M KCl inside the pore (along with either 500 pM λ-DNA or 500 pM 10 kbp DNA) and 4 M KCl outside the pore, current enhancements were produced at negative voltages (i.e., electrophoresis drives DNA out of the pore). Based on TEM images of nanopipettes pulled using the same protocol (**see Supplemental Information**), we estimate that the pore size for both experiments was approximately 20 nm. Translocation data was collected at a voltage bias of -400 mV for both DNA analytes and the current enhancements were 223 ± 35 pA and 235 ± 47 pA for λ-DNA and 10 kbp DNA, respectively (see Supporting Information). The dwell times at the same voltage condition were most different and had a more bimodal distribution. The most notable difference was that the peak corresponding to the fastest dwell times was located at 2.2 ms for λ-DNA and 251 μs 10 kbp DNA, respectively (see Supporting Information). Given that λ-DNA is 48.5 kbp, it is not surprising that 10 kbp would have such a short dwell time within the pore.

Exponential fitting of each event signature's rise and fall yielded nearly identical decay rates (924 s^{-1} for the event rise and 910 s^{-1} for the event fall) based on the peak of the gaussian

fits (**Fig. 6b**). The decay rates for both the event rise and event fall were nearly the same and was unique to asymmetric salt; this was not the case for 10 mM KCl where the decay rate was higher for the event rise compared to the event fall. Since the Debye length is larger at 10 mM KCl compared to 1 M KCl, we suspect that surface charge phenomena may be important to sensing the capacitance change due to a molecule. The second interesting observation is that the value of the decay rates is much smaller (i.e., takes longer to decay) than 10 mM KCl. The lower decay rate suggests that there is also a lower lowpass cutoff frequency (F_{LP}) associated with these recordings. With the RC time constant being the inverse of the decay rate, and using $\tau = \frac{T_r}{2.2}$, the T_r is 2.4 ms which yields a $T_{critical}$ of 4.8 ms. Using the relationship $T_r = \frac{0.35}{F_{LP}}$ and solving for F_{LP}, we obtain an effective lowpass cutoff frequency of 146 Hz. Plotting the theoretical attenuation curves along with the DNA event properties (scatter plot of dwell time and current enhancement), there is a general agreement between the experimental data and the bandwidth calculations.

The extraordinarily low F_{LP} values found here are far below the instrument bandwidth (10 kHz in all experiments). The ionic filtering effect therefore may limit the detection capabilities of certain experiments; namely those producing conductive events. Smaller molecules like protein are most susceptible to bandwidth limitations since they tend to translocate much faster. The 10 kbp DNA translocations were analyzed and fitted using the same procedure as the λ-DNA. The decay rates were much faster compared to the λ-DNA with a peak decay rate of 7382 s^{-1} for 10kbp DNA (**Fig. 6d**). The higher decay rate means that smaller molecules have a higher effective bandwidth which is beneficial to sensing. Only the event fall could be fitted however since the initial moments of the event lacked a clear exponential rise. Using a decay rate of 7382 s^{-1}, the calculated $T_{critical}$ was found to be 596 µs. Since nearly all the events for 10 kbp DNA had a dwell time less than 596 µs, we suspect that most of the events were attenuated. The attenuation of events is likely the reason that the rising edge of the event could not be fitted to an exponential (i.e., the event never reached the fully blocked current state).

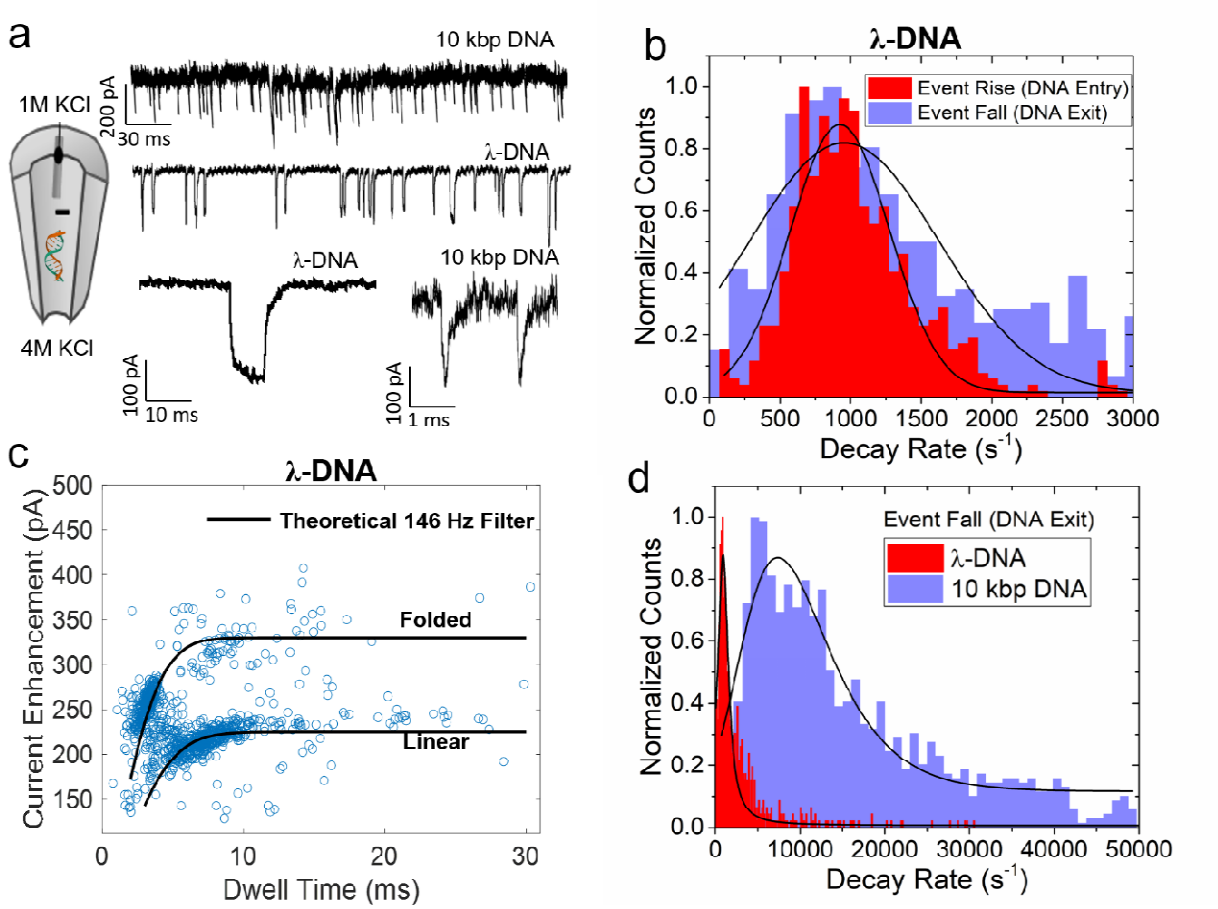

Fig. 6 (a) Current traces showing 10 kbp DNA and λ-DNA events collected under asymmetric salt conditions (1 M/4 M KCl, pH 7.4). All events were collected at a negative voltage bias (-400 mV) and events were conductive. (b) Decay rate histogram for both the event rise and fall which corresponds to the DNA entering the pore and exiting the pore, respectively. (c) Scatter plot of λ-DNA event properties and a theoretical lowpass filter with a cutoff frequency of 146 Hz. (d) Histogram of the event fall (DNA exit) decay rate for λ-DNA and 10 kbp-DNA. All data was collected at a voltage bias of -400 mV.

Conclusion

It was stated previously that the three possible scenarios which could explain negative capacitance were: (1) C<0, (2) — , (3) — . Although C<0 could explain the IV recordings, we remain skeptical that negative capacitance can explain the translocation data. The

reason being that during a translocation event, the initial decay towards the new equilibrium (i.e., blocked state) produced a current transient that added a positive current contribution whereas the tail of the event (i.e. towards the open pore state) had a current transient that added a negative current contribution. The only way that such current transients can be possible is if there is pulse-like change in either the capacitance of the pore, the voltage of the pore, or both. Using the current equations for Model 1 and Model 2, we further found that (1) capacitance must decrease during a translocation event and/or (2) the voltage magnitude must decrease during a translocation event (**see Supplemental Information**). This observation can also be made by looking at the signs of each term in Figure 1f-g (assuming capacitance is positive). Only these two situations would produce current transients that would add to the "pulse-like" nature of the event to produce the decays seen here. We also believe that building a new circuit model will help explain the data presented here. A Warburg element, typically placed in series with a resistor, can capture diffusion processes within an electrochemical system and may provide more information about the correct equivalent circuit (**see Supplemental Information** for more detail). A purely resistive change due to molecular occupancy of the pore, however, seems to be the least fitting model to explain the data shown here. A Warburg impedance, however, in series with the nanopore would provide a mechanism for voltage fluctuations at the pore and would vary depending on the degree of concentration polarization ($V_{applied} = V_{pore} + V_{polarization}$).

Although negative capacitance has been reported in simulations[27,46,47], and sometimes experimentally in solar cell characterization[30,48], this report is the first to study the unique effects negative capacitance within nanopores, and ionic storage phenomenon on single molecule events. The appearance of negative capacitance effects has previously been attributed to out-of-phase charge recombination which alludes to two ionic effects occurring at different timescales. Ionic charge and the migration of charge at interfaces also have been proposed to be fundamentally linked to the phenomenon. Here, charge accumulation at the glass-electrolyte interface, in combination with hindered diffusion/dissipation of ions, is hypothesized to be a critical factor. Due to the tapered geometry of the nanopore (i.e., a nanopipette), any excess charge accumulation in the taper will experience virtually one dimensional, hindered diffusion with high interactions with the glass wall. We further want to point out that all events recorded here were conductive in nature and therefore there may exist a link between conductive events and non-linear electrokinetics. Negative capacitance as well as the time constant associated with

single molecule events could not be replicated in numerical models based on Poisson-Nernst-Planck and Navier-Stokes equations and so the results of those models were not included here. Furthermore, although planar membrane nanopores have not been explored here, we suspect they would yield different charging/discharging properties, or the same effects will not be observed at all.

Methods

Nanopipette Fabrication

Quartz capillaries (Sutter Instruments, 1 mm outer diameter, 0.7 mm inner diameter) were pulled by a Sutter P2000 laser pipette puller. A relationship between conductance (using 10 mM salt) and pore size (via transmission electron microscopy: TEM) was used for nanopore sizing. See Supplemental Information for TEM images and corresponding conductance values.

IV- and Gap-free Ionic Current Recordings

Current-Voltage (IV) relationships were recorded using an Axopatch 200B amplifier (Molecular Devices) and pClamp software. The IV protocol used episodic stimulation wherein the voltage sweeps started at zero voltage and initiated a voltage step at approximately 2 seconds. The duration of the file was adjusted to capture the dissipation of capacitive current. For IV curves that applied -1000 to +1000 mV, each sweep was extended to 10 seconds whereas IV curves which applied -500 to +500 mV, the sweep length was only 5.5 seconds. All IV curves started at the maximum negative voltage and made increments towards the positive voltage bias. All voltages are referenced to the outside of the nanopipette (i.e., bath). The buffer used in all experiments, unless otherwise noted, was Tris:HCl with EDTA. For the IV curves conducted at pH 10, CAPS buffer was used instead of Tris. The λ-DNA and 10 kbp DNA used in experiments was obtained from New England BioLabs.

Event Detection

The λ-DNA events were detected using custom MATLAB code which detects events based on a threshold value (the threshold was kept constant and was set as a multiple of the standard deviation of the background). The dwell time was measured as the full-width-half-max (FWHM)

of the event signature. For example, if an event induced a current change of 100 pA (i.e., peak current change), the time points where the event reached 50 pA current modulation were used to find the dwell time. All current enhancement values were the peak current enhancement of each event. No additional filtering of the events was done after event detection.

Exponential Fitting and Time Constant Extraction

The time constants associated with a voltage switch as well as the DNA events were fitted by a single exponential of the form: $\Delta I = Ce^{-rt}$, where C and r are fitting constants. If the exponential shape of the current transient was anything other than a positive current decaying towards zero, the signals were flipped (multiplied by -1) and the equilibrium current value was subtracted. All fits were checked for goodness of fit (R^2>0.95). Unless otherwise noted, the first 20 ms of data (post voltage switch) were used for fitting. For fitting of DNA rise times (i.e., the beginning of the event), the initial data point was the first FWHM point. The subsequent 0.8 ms of the event was then fitted to the exponential ($\Delta I = Ce^{-rt}$) after subtracting the equilibrium value such that the current decayed to zero. Prior to this, only events >1 ms were used to ensure that 0.8 ms of data was obtainable for accurate fitting. For fitting the DNA fall times (i.e., the end of the event), the second FWHM point was used as the initial data point. The subsequent 0.8 ms of data was then used for fitting. An illustration of the FWHM points used in the event rise and fall fittings are shown in the **Supplemental Information**.

Acknowledgements

This work was supported by the Human Frontier Science Program (RGY0066/2018).

Competing interests

The authors have no competing interests.

Data availability

The data that support the findings of this study are available from the corresponding author upon request.

Code availability

The code used to analyze data in this study are available from the corresponding author upon request.

References

1 Mishchuk, N. A. Concentration polarization of interface and non-linear electrokinetic phenomena. *Advances in Colloid and Interface Science* **160**, 16-39 (2010).

2 Schlaich, A., Jin, D., Bocquet, L. & Coasne, B. Electronic screening using a virtual Thomas–Fermi fluid for predicting wetting and phase transitions of ionic liquids at metal surfaces. *Nature materials* **21**, 237-245 (2022).

3 Green, Y. Ion transport in nanopores with highly overlapping electric double layers. *The Journal of Chemical Physics* **154**, 084705 (2021).

4 Liu, F.-F., Zhao, X.-P., Kang, B., Xia, X.-H. & Wang, C. Non-linear mass transport in confined nanofluidic devices for label-free bioanalysis/sensors. *TrAC Trends in Analytical Chemistry* **123**, 115760 (2020).

5 Guerrero-García, G. I., Gonzalez-Tovar, E., Chávez-Páez, M. & Wei, T. Expansion and shrinkage of the electrical double layer in charge-asymmetric electrolytes: A non-linear Poisson-Boltzmann description. *Journal of Molecular Liquids* **277**, 104-114 (2019).

6 Levitan, J. A. *et al.* Experimental observation of induced-charge electro-osmosis around a metal wire in a microchannel. *Colloids and Surfaces A: Physicochemical and Engineering Aspects* **267**, 122-132 (2005).

7 Squires, T. M. Induced-charge electrokinetics: fundamental challenges and opportunities. *Lab on a Chip* **9**, 2477-2483 (2009).

8 Bazant, M. Z., Kilic, M. S., Storey, B. D. & Ajdari, A. Towards an understanding of induced-charge electrokinetics at large applied voltages in concentrated solutions. *Advances in colloid and interface science* **152**, 48-88 (2009).

9 Burger, M., Schlake, B. & Wolfram, M.-T. Nonlinear Poisson–Nernst–Planck equations for ion flux through confined geometries. *Nonlinearity* **25**, 961 (2012).

10 Dreyer, W., Guhlke, C. & Müller, R. Overcoming the shortcomings of the Nernst–Planck model. *Physical Chemistry Chemical Physics* **15**, 7075-7086 (2013).

11 Doblhoff-Dier, K. & Koper, M. T. Modeling the Gouy–Chapman diffuse capacitance with attractive ion–surface interaction. *The Journal of Physical Chemistry C* **125**, 16664-16673 (2021).

12 Yao, Y., Wen, C., Pham, N. H. & Zhang, S.-L. On induced surface charge in solid-state nanopores. *Langmuir* **36**, 8874-8882 (2020).

13 Bazant, M. Z., Thornton, K. & Ajdari, A. Diffuse-charge dynamics in electrochemical systems. *Physical review E* **70**, 021506 (2004).

14 Zhang, L.-X., Cao, X.-H., Cai, W.-P. & Li, Y.-Q. Observations of the effect of confined space on fluorescence and diffusion properties of molecules in single conical nanopore channels. *Journal of fluorescence* **21**, 1865-1870 (2011).

15 Paulsen, B. D., Tybrandt, K., Stavrinidou, E. & Rivnay, J. Organic mixed ionic–electronic conductors. *Nature materials* **19**, 13-26 (2020).

16 Jash, P., Parashar, R. K., Fontanesi, C. & Mondal, P. C. The Importance of Electrical Impedance Spectroscopy and Equivalent Circuit Analysis on Nanoscale Molecular Electronic Devices. *Advanced Functional Materials*, 2109956 (2021).

17 Hyun, C., Rollings, R. & Li, J. Probing access resistance of solid-state nanopores with a scanning-probe microscope tip. *small* **8**, 385-392 (2012).

18 Heins, E. A., Siwy, Z. S., Baker, L. A. & Martin, C. R. Detecting single porphyrin molecules in a conically shaped synthetic nanopore. *Nano letters* **5**, 1824-1829 (2005).
19 Wanunu, M., Morrison, W., Rabin, Y., Grosberg, A. Y. & Meller, A. Electrostatic focusing of unlabelled DNA into nanoscale pores using a salt gradient. *Nature nanotechnology* **5**, 160-165 (2010).
20 Wen, C. *et al.* Generalized noise study of solid-state nanopores at low frequencies. *ACS sensors* **2**, 300-307 (2017).
21 Smeets, R. M., Keyser, U. F., Dekker, N. H. & Dekker, C. Noise in solid-state nanopores. *Proceedings of the National Academy of Sciences* **105**, 417-421 (2008).
22 Lee, M.-H. *et al.* A low-noise solid-state nanopore platform based on a highly insulating substrate. *Scientific reports* **4**, 1-7 (2014).
23 Ma, J. *et al*. Drastically reduced ion mobility in a nanopore due to enhanced pairing and collisions between dehydrated ions. *Journal of the American Chemical Society* **141**, 4264-4272 (2019).
24 Li, Z., Qiu, Y., Zhang, Y., Yue, M. & Chen, Y. Effects of surface trapping and contact ion pairing on ion transport in nanopores. *The Journal of Physical Chemistry C* **123**, 15314-15322 (2019).
25 Lin, C.-Y., Yeh, L.-H. & Siwy, Z. S. Voltage-induced modulation of ionic concentrations and ion current rectification in mesopores with highly charged pore walls. *The journal of physical chemistry letters* **9**, 393-398 (2018).
26 Khan, M. T., Huang, P., Almohammedi, A., Kazim, S. & Ahmad, S. Mechanistic origin and unlocking of negative capacitance in perovskites solar cells. *Iscience* **24**, 102024 (2021).
27 Krems, M., Pershin, Y. V. & Di Ventra, M. Ionic memcapacitive effects in nanopores. *Nano letters* **10**, 2674-2678 (2010).
28 Klausen, L. H., Fuhs, T. & Dong, M. Mapping surface charge density of lipid bilayers by quantitative surface conductivity microscopy. *Nature communications* **7**, 1-10 (2016).
29 Gupta, A., Zuk, P. J. & Stone, H. A. Charging dynamics of overlapping double layers in a cylindrical nanopore. *Physical review letters* **125**, 076001 (2020).
30 Ebadi, F., Taghavinia, N., Mohammadpour, R., Hagfeldt, A. & Tress, W. Origin of apparent light-enhanced and negative capacitance in perovskite solar cells. *Nature communications* **10**, 1-9 (2019).
31 Kumar, R. *et al.* Unveiling the morphology effect on the negative capacitance and large ideality factor in perovskite light-emitting diodes. *ACS Applied Materials & Interfaces* **12**, 34265-34273 (2020).
32 Brown, W., Kvetny, M., Yang, R. & Wang, G. Selective Ion Enrichment and Charge Storage through Transport Hysteresis in Conical Nanopipettes. *The Journal of Physical Chemistry C* **126**, 10872-10879 (2022).
33 Li, Y. *et al.* History-dependent ion transport through conical nanopipettes and the implications in energy conversion dynamics at nanoscale interfaces. *Chemical science* **6**, 588-595 (2015).
34 Wang, D. *et al.* Hysteresis charges in the dynamic enrichment and depletion of ions in single conical nanopores. *ChemElectroChem* **5**, 3089-3095 (2018).
35 Levy, A., de Souza, J. P. & Bazant, M. Z. Breakdown of electroneutrality in nanopores. *Journal of Colloid and Interface Science* **579**, 162-176 (2020).
36 Voukadinova, A. & Gillespie, D. Energetics of counterion adsorption in the electrical double layer. *The Journal of chemical physics* **150**, 154706 (2019).
37 Matse, M., Berg, P. & Eikerling, M. Asymmetric double-layer charging in a cylindrical nanopore under closed confinement. *The journal of chemical physics* **152**, 084103 (2020).
38 Lastra, L. S., Bandara, Y., Nguyen, M., Farajpour, N. & Freedman, K. J. On the origins of conductive pulse sensing inside a nanopore. *Nature Communications* **13**, 1-11 (2022).

39 Yossifon, G., Mushenheim, P., Chang, Y.-C. & Chang, H.-C. Nonlinear current-voltage characteristics of nanochannels. *Physical Review E* **79**, 046305 (2009).
40 Bakhshandeh, A., Segala, M. & Colla, T. Electrolytes in regimes of strong confinement: surface charge modulations, osmotic equilibrium and electroneutrality. *Soft Matter* **16**, 10488-10505 (2020).
41 de Souza, J. P., Levy, A. & Bazant, M. Z. Electroneutrality breakdown in nanopore arrays. *Physical Review E* **104**, 044803 (2021).
42 García-Sánchez, P., Ramos, A., Gonzalez, A., Green, N. G. & Morgan, H. Flow reversal in traveling-wave electrokinetics: An analysis of forces due to ionic concentration gradients. *Langmuir* **25**, 4988-4997 (2009).
43 Biesheuvel, P. & Van Soestbergen, M. Counterion volume effects in mixed electrical double layers. *Journal of Colloid and Interface Science* **316**, 490-499 (2007).
44 Carlsen, A. T., Zahid, O. K., Ruzicka, J., Taylor, E. W. & Hall, A. R. Interpreting the conductance blockades of DNA translocations through solid-state nanopores. *Acs Nano* **8**, 4754-4760 (2014).
45 Zhang, Y. *et al.* Ionic current modulation from DNA translocation through nanopores under high ionic strength and concentration gradients. *Nanoscale* **9**, 930-939 (2017).
46 Wang, D. *et al.* Transmembrane potential across single conical nanopores and resulting memristive and memcapacitive ion transport. *Journal of the American Chemical Society* **134**, 3651-3654 (2012).
47 Mandal, S. DNA in Nanopores: Negative Capacitance and ▪ -Relaxation at High Frequency. *Journal of nanoscience and nanotechnology* **6**, 1453-1457 (2006).
48 Alvarez, A. O. *et al.* Negative capacitance and inverted hysteresis: Matching features in perovskite solar cells. *The journal of physical chemistry letters* **11**, 8417-8423 (2020).